ChemComm

COMMUNICATION

View Article Online
View Journal | View Issue

Cite this: *Chem. Commun.*, 2016, 52, 4199

Received 2nd January 2016,
Accepted 17th February 2016

DOI: 10.1039/c6cc00011h

www.rsc.org/chemcomm

A metal–organic framework-templated synthesis of γ-Fe_2O_3 nanoparticles encapsulated in porous carbon for efficient and chemoselective hydrogenation of nitro compounds†

Yang Li,‡ Yu-Xiao Zhou,‡ Xiao Ma and Hai-Long Jiang*

The γ-Fe_2O_3 nanoparticles well dispersed in porous carbon were fabricated *via* a Fe-based metal–organic framework-templated pyrolysis. The resultant product exhibits excellent catalytic activity, chemoselectivity and magnetic recyclability for the hydrogenation of diverse nitro compounds under mild conditions.

Aromatic amines, primarily prepared *via* the reduction of aromatic nitro compounds, are important feedstocks and key intermediates for the manufacture of dyes, pigments, agrochemicals, herbicides, pharmaceuticals and fine chemicals.[1] Due to the growing environmental concern, hydrazine hydrate ($N_2H_4{\cdot}H_2O$) should be a suitable reducing agent for this transformation, generating only N_2 as a byproduct, which minimizes the influence on the surrounding environment and the purity of the resultant anilines. On the other hand, although RANEY® Ni has been demonstrated to be effective for the reduction of simple nitroarenes, the hydrogenation of their functionalized substrates usually relies on noble metal-based catalysts (for example, Ru, Pt, Pd, *etc.*).[2] The high price and scarcity of these precious metals greatly limit their large-scale industrial applications. Moreover, the presence of other reducible functional groups in the nitroarenes makes the selective reduction especially for a nitro group quite challenging. In addition to the supported Au nanocatalysts,[3] most of precious metals are usually not chemoselective; the modification by suitable additives onto the catalysts allows the improvement of the selectivity. However, that requires additional synthetic treatments and the additives also cause environmental issues.[4] As an alternative choice, the heterogeneous catalysts based on base metals (for examples, Fe, Co, and Ni), are earth-abundant and cost-effective, while their leaching and sintering readily cause irreversible activity drop in reaction solutions.[5]

To obtain efficient and stable base metal-based catalysts, the encapsulation of highly dispersed metal/metal oxide nanoparticles (NPs) inside the porous host materials would be an effective solution. In this context, metal–organic frameworks (MOFs),[6] a class of crystalline porous materials with diversified and tailorable structures, have been demonstrated to be ideal templates/precursors to afford uniform and small metal and/or metal oxide NPs distributed throughout the porous carbon matrix.[7] Although the synthesis and multifunctionalities of MOF-derived composites have been extensively reported, their application in catalysis were relatively rare.[7] Given that Fe-based nanocatalysts are abundant, eco-friendly, inexpensive and magnetically recyclable, the Fe_2O_3 species active for hydrogenation of nitroarenes are considered to be suitable candidates.[5c]

With these in mind, a representative Fe-based MOF, $Fe_3O(FA)_3(H_2O)_2(NO_3)$ (called Fe-MIL-88A, FA = fumaric acid),[8] in a spindle shape was synthesized. The Fe-MIL-88A microcrystals as templates/precursors were converted to magnetic γ-Fe_2O_3 nanoparticles (NPs) embedded in porous carbon *via* one-step facile pyrolysis at 500 °C. The resultant product was found to be highly efficient, chemoselective and magnetically recyclable for the hydrogenation of various nitro compounds to anilines under mild conditions using hydrazine hydrate as the reductant (Scheme 1). To the best of our knowledge, this is the first work on the transfer hydrogenation of nitro compounds over MOF-derived nanocomposites.

The Fe-MIL-88A was solvothermally synthesized based on $Fe(NO_3)_3{\cdot}9H_2O$ and fumaric acid in DMF solution.[8] The structure of Fe-MIL-88A features a 3D network with hexagonal channels composed of trimers of FeO_6 octahedra linked by fumarates. The phase purity of Fe-MIL-88A has been confirmed by powder X-ray diffraction (XRD) (Fig. S1, ESI†). The obtained Fe-MIL-88A samples were thermally treated at different temperatures (from 500 to 700 °C) in a N_2 atmosphere to afford Fe-based NPs encapsulated inside porous carbon, denoted as Fe-*T*-*t* (*T* and *t* represent pyrolysis temperature and time, respectively; *T* = 500, 600, 700; *t* = 1 h, 2 h, 3 h). As indicated by powder XRD patterns, the composition

Hefei National Laboratory for Physical Sciences at the Microscale, CAS Key Laboratory of Soft Matter Chemistry, Collaborative Innovation Center of Suzhou Nano Science and Technology, Department of Chemistry, University of Science and Technology of China, Hefei, Anhui 230026, P. R. China.
E-mail: jianglab@ustc.edu.cn

† Electronic supplementary information (ESI) available: Detailed experimental procedures and supporting figures. See DOI: 10.1039/c6cc00011h

‡ These authors contributed equally to this work.

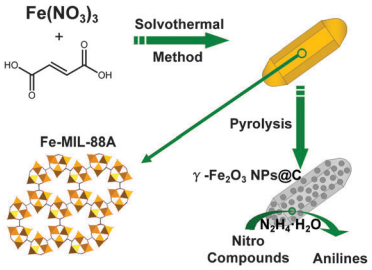

Scheme 1 Schematic illustration of the synthesis of porous carbon encapsulated γ-Fe_2O_3 NPs templated by Fe-MIL-88A.

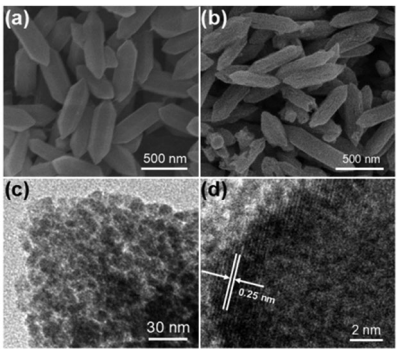

Fig. 1 Microstructure observation for Fe-MIL-88A and Fe-500-1 h. (a) SEM images of (a) Fe-MIL-88A and (b) Fe-500-1 h. (c) TEM and (d) HRTEM images of Fe-500-1 h.

of the products obtained at different temperatures displays distinct differences (Fig. S2, ESI†). All peaks for Fe-500-1 h can be identified and indexed to the phase of maghemite (γ-Fe_2O_3, JCPDS NO. 39-1346),[9a] in which the broad peaks could be caused by the small sizes of Fe_2O_3 NPs. In contrast, the diffraction peaks become much sharper in Fe-600-1 h and Fe-700-1 h samples, revealing the presence of larger particles. For Fe-600-1 h, the strongest peaks can be indexed to α-Fe (JCPDS NO. 06-0696), while some relatively weak peaks are assignable to γ-Fe_2O_3 and Fe_3C (JCPDS NO. 35-0772).[9b] In Fe-700-1 h, α-Fe is still the major product, accompanied by more portions of Fe_3C while no sign of γ-Fe_2O_3 can be found. Moreover, the powder XRD patterns of Fe-500-2 h and Fe-500-3 h give only α-Fe and Fe_3C, but do not contain the γ-Fe_2O_3 species. These results unambiguously suggest the possible reduction of Fe_2O_3 to Fe or/and Fe_3C species at temperatures higher than 500 °C or with longer time of pyrolysis. The inductively coupled plasma mass spectrometry (ICP-MS) results show that the Fe contents are 21.99%, 25.99%, and 30.92%, respectively for Fe-500-1 h, Fe-600-1 h and Fe-700-1 h (Table S1, ESI†), which is understandable as some γ-Fe_2O_3 have been reduced to α-Fe or Fe_3C at higher temperatures, in agreement with powder XRD results. The pore character and surface areas of pyrolysis products were characterized by N_2 sorption measurements at 77 K. They partially inherit the porosity of the MOF although the samples obtained at different temperatures have distinct sorption features (Fig. S3a, ESI†). The pore size distribution analysis suggests that Fe-500-1 h possesses hierarchical pores (Fig. S3b, ESI†), which would allow the exposure of active sites as far as possible, limit the migration and aggregation of the active NPs, and also facilitate the transportation of catalytic substrates and products.

The microstructure observation using scanning electron microscopy (SEM) suggests that Fe-MIL-88A microcrystals are of uniform spindle shape and with a length of ~700 nm (Fig. 1a). After pyrolysis, taking Fe-500-1 h as the representative, its shape is almost retained while the size is reduced to some extent (length: ~600 nm, Fig. 1b). A small number of spindles have been broken, possibly caused by the rapid shrinking during pyrolysis (Fig. 1b). As shown in the transmission electron microscope (TEM) image for Fe-500-1 h, high-density small NPs (6–10 nm) are uniformly distributed throughout the porous carbon (Fig. 1c, Fig. S4, ESI†). The high-resolution TEM (HRTEM) image displays clear lattice fringe, suggesting the good crystallinity. The 0.25 nm interplanar crystal spacing corresponds to the (311) crystal plane of γ-Fe_2O_3, further demonstrating the formation of γ-Fe_2O_3 inside the porous carbon (Fig. 1d).

To further understand the existing form of the Fe species, taking Fe-500-1 h as the representative, investigation using X-ray photoelectron spectroscopy (XPS) has been carried out. As shown in Fig. S5 (see ESI†), the Fe 2p exhibits two broad peaks at 723.9 and 710.3 eV, assigned to Fe $2p_{1/2}$ and Fe $2p_{3/2}$, respectively. Their separation $\Delta = 2p_{1/2} - 2p_{3/2} = 13.6$ eV is very similar to that reported for γ-Fe_2O_3,[8,10] which is also supported by the powder XRD results given above. Additionally, the characteristic satellite peak at 719.6 eV for γ-Fe_2O_3 is also observed. All these characterizations clearly suggest that the direct pyrolysis of Fe-MIL-88A at 500 °C leads to the incorporation of well-dispersed crystalline γ-Fe_2O_3 NPs in porous carbon.

We are now in a position to investigate the catalytic performance of MOF-pyrolyzed Fe-*T*-*t* in the hydrogenation of nitroarenes in the presence of hydrazine hydrate as the reducing agent. Nitrobenzene as the model substrate was first used to explore the optimized reaction conditions and also the catalytic activity of different catalysts (Table 1). Among different pyrolysis temperatures, the activity of the obtained catalysts gradually decreases with elevated pyrolysis temperatures from 500 °C to 700 °C. As a result, the catalyst pyrolyzed at 500 °C for 1 h (Fe-500-1 h) gives the best activity (entries 1–3). It seems that the prolonged pyrolysis time is also not beneficial for the activity (entries 4 and 5). Therefore, it is safe to conclude that γ-Fe_2O_3 as the component of Fe-500-1 h is more active than the α-Fe or Fe_3C species obtained at higher temperatures or longer pyrolysis time. Despite this, the γ-Fe_2O_3 species supported on active carbon is active but it takes a longer reaction time to achieve complete conversion than that of Fe-500-1 h (entry 6, Fig. S6, ESI†). As-synthesized Fe-MIL-88A shows low activity in the reduction of nitrobenzene to aniline (entry 7), and it is actually unstable in the presence of hydrazine hydrate. In the absence of catalyst or reducing agent (hydrazine hydrate), the hydrogenation of nitrobenzene cannot proceed (entries 8 and 9). These results suggest that the special structure of Fe-500-1 h with high-density active γ-Fe_2O_3 sites well accessible to the substrate through the porous carbon matrix could play crucial roles in the high catalytic activity.

Table 1 The catalytic reduction of nitrobenzene to aniline with different catalysts[a]

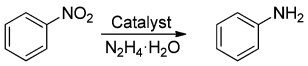

Entry	Catalyst	Time (h)	Yield[c] (%)
1	Fe-700-1 h	4	35.4
2	Fe-600-1 h	2	36.9
3	Fe-500-1 h	1	100
4	Fe-500-2 h	1.5	98.0
5	Fe-500-3 h	2.5	98.8
6	γ-Fe_2O_3/C	3	100
7	MIL-88A	6	7.5
8	No catalyst	12	0
9[b]	Fe-500-1 h	12	0

[a] Reaction conditions: 1 mmol nitrobenzene, 0.025 mmol Fe-based catalyst, 4 mmol hydrazine hydrate, and 5 mL alcohol, reflux at 85 °C otherwise mentioned. [b] Without hydrazine hydrate. [c] Determined by GC and using *n*-dodecane as the standard.

To demonstrate the stability and reusability of Fe-500-1 h, recycling experiments for the hydrogenation of nitrobenzene were conducted. As shown in Fig. 2a, both catalytic activity and chemoselectivity were very well retained in the ten consecutive runs. TEM observation clearly demonstrated the maintained NP size and shape of the catalyst after recycling (Fig. S7, ESI†), suggesting its great stability and recyclability. To verify the nature of the Fe-500-1 h catalyst, the hot filtration test was carried out from the mixture after 30 min of reaction, no further conversion of nitrobenzene was observed even after 2 hours of reaction under identical conditions, leading to the inference that no leaching of the catalyst occurred and the process is truly heterogeneous (Fig. 2b). In addition, the catalyst was easily separated by an external magnet due to the strong magnetism of γ-Fe_2O_3 (Fig. 2b, inset). Therefore, the Fe-500-1 h catalyst presents an impressive catalytic activity and recyclability, and possesses a truly heterogeneous catalytic nature, showing potential application in the chemical industry.

Encouraged by the superb performance of Fe-500-1 h, a variety of functionalized nitro compounds were investigated. As shown in Table 2, most of the corresponding substituted anilines were obtained with high conversion and selectivity. Notably, halogen-substituted nitroarenes were effectively reduced to the corresponding haloaromatic amines without obvious dehalogenation (entries 1–7). Furthermore, the high performance

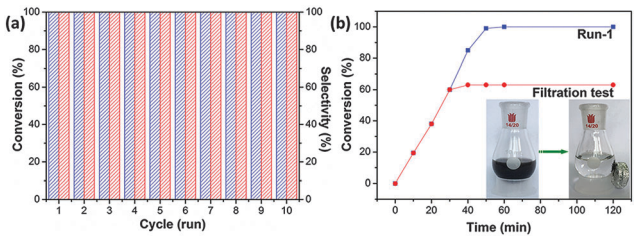

Fig. 2 (a) Conversion (blue column) and selectivity (red column) of ten consecutive runs and (b) hot filtration test of the reduction of nitrobenzene with Fe-500-1 h as a catalyst. Inset of (b): The photographs showing the facile separation of the catalyst *via* an external magnet.

Table 2 The catalytic hydrogenation of both aromatic and aliphatic nitro compounds to their amines with Fe-500-1 h[a]

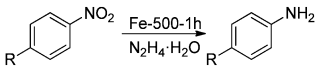

Entry	Substrate	Time (h)	Conv.[d] (%)	Select.[d] (%)
1	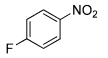	1.5	100	99
2	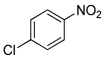	1.5	100	98
3	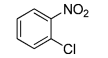	0.75	100	100
4	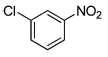	6	81	96.7
5	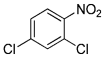	0.75	100	>98
6	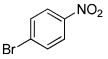	1.25	100	100
7[b]	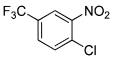	2	100	100
8	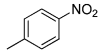	1.5	100	100
9[b]	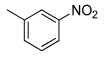	6	100	100
10[b]	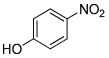	6	100	100
11	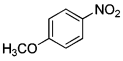	2	100	100
12	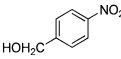	5	100	100
13[b]	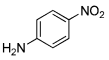	4	100	100
14[b]	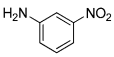	1.5	100	100
15	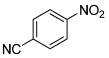	2	98	100
16[c]	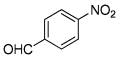	2	100	98
17	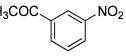	6	100	100
18[b]	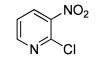	12	62	100
19[b]	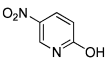	12	69	100
20	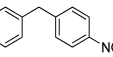	8	100	100
21	CH_3NO_2	1	100	100
22	$CH_3CH_2NO_2$	2	81	100

[a] Reaction conditions: 1 mmol substrate, 4 mmol hydrazine hydrate, 0.025 mmol catalyst, 5 mL alcohol, reflux at 85 °C otherwise mentioned. [b] 5 mL CH_3CN was substituted for alcohol. [c] 5 mL DMF was substituted for alcohol. [d] Determined by GC using *n*-dodecane as the standard.

was obtained in the hydrogenation of methyl-substituted nitrobenzenes with 100% conversion and 100% selectivity (entries 8 and 9). This catalyst also showed absolute selectivity in the reduction of nitroarenes in the presence of other functional

groups, including amino, phenolic hydroxyl and alcoholic hydroxyl, and no byproduct was detectable (entries 10–14). To our delight, the Fe-500-1 h was also able to offer a high chemoselectivity in the reduction of substituted nitroarenes with quite challenging reducible functional groups, including nitrile, aldehyde and ketone (entries 15–17), giving the only product of corresponding anilines while the reducible functional groups were unchanged. This result further highlights the chemoselectivity of this γ-Fe_2O_3-based nanocatalyst, displaying remarkable advantage compared to that of noble metal-based catalysts. Moreover, the hydrogenation of heteroaromatic nitro compounds was also investigated, among which although the reduction of 2-chloro-3-nitropyridine and 2-hydroxy-5-nitropyridine were relatively slow (62% and 69% conversion in 12 h, respectively), the reaction selectivity for all substrates is as high as 100% (entries 18–20). In addition to the efficient and chemoselective conversion for the reduction of substituted nitroarenes above, we turned our interest towards aliphatic nitro compounds (entries 21 and 22). In the presence of Fe-500-1 h, aliphatic nitro compounds were capable of being reduced to the corresponding aliphatic amines with high conversion, again manifesting that the Fe-500-1 h is effective for the hydrogenation of diverse substrates, both aromatic and aliphatic nitro compounds.

Based on the above results, a possible three-step mechanism for the reduction of nitrobenzene catalyzed by γ-Fe_2O_3 NPs encapsulated in porous carbon can be proposed (Scheme S1, ESI†).[5d] Nitrobenzene is firstly reduced to nitrosobenzene, and then rapidly converted to phenylhydroxylamine. The above two steps possess fast reaction kinetics. Finally, the intermediate transforms directly to final product and this step is considered to be the rate-determining step. Moreover, the Fe-500-1 h catalyst featuring hierarchical pores, as demonstrated by the pore size analysis (Fig. S3b, ESI†), might facilitate the transportation of substrates, intermediates and products. In this case, diverse functionalized nitro compounds can be reduced to the corresponding amines under mild conditions.

In summary, we have developed a highly efficient, low-cost, and magnetically recyclable γ-Fe_2O_3@porous carbon nanocatalyst for the hydrogenation of nitro compounds, *via* a facile pyrolysis of a representative MOF, Fe-MIL-88A. The small γ-Fe_2O_3 NPs are well dispersed inside the porous carbon, which effectively limits the aggregation and growth of the high-density NPs with an average size of *ca.* 6–10 nm and facilitates the transportation of substrates, intermediates and products. Remarkably, this non-noble metal oxide-based nanocomposite behaves as an efficient and stable catalyst for the hydrogenation of a variety of substituted aromatic or aliphatic nitro compounds, into their corresponding amines. More importantly, in addition to the tolerance to general groups, the catalyst exhibits high chemoselectivity to the reducible groups, including nitrile, aldehyde and ketone. The γ-Fe_2O_3-based nanocatalyst is readily recycled with an external magnet and can be reused at least 10 times without any loss of activity. This study provides a versatile platform based on MOFs to introduce highly dispersed active metal/metal oxide species inside the porous carbon matrix with targeted and improved performance toward diverse catalytic reactions.

This work was supported by the NSFC (21371162, 51301159 and 21521001), the 973 program (2014CB931803), NSF of Anhui Province (1408085MB23), the Recruitment Program of Global Youth Experts and the Fundamental Research Funds for the Central Universities (WK2060190026).

Notes and references

1 (*a*) N. Ono, *The Nitro Group in Organic Synthesis*, Wiley-VCH, New York, 2001; (*b*) R. S. Downing, P. J. Kunkeler and H. van Bekkum, *Catal. Today*, 1997, **37**, 121; (*c*) H.-U. Blaser, H. Steiner and M. Studer, *ChemCatChem*, 2009, **1**, 210.
2 (*a*) S. Nishimura, *Heterogeneous Catalytic Hydrogenation*, John Wiley & Sons, 2001; (*b*) B. Cornils and W. A. Herrmann, *Applied Homogeneous Catalysis with Organometallic Compounds*, Wiley-VCH, Weinheim, Germany, 2nd edn, 2002.
3 (*a*) A. Corma and P. Serna, *Science*, 2006, **313**, 332; (*b*) A. Grirrane, A. Corma and H. García, *Science*, 2008, **322**, 1661; (*c*) S.-C. Li and U. Diebold, *J. Am. Chem. Soc.*, 2010, **132**, 64; (*d*) X. Liu, H.-Q. Li, S. Ye, Y.-M. Liu, H.-Y. He and Y. Cao, *Angew. Chem., Int. Ed.*, 2014, **53**, 7624.
4 (*a*) A. Corma, P. Serna, P. Concepción and J. J. Calvino, *J. Am. Chem. Soc.*, 2008, **130**, 8748; (*b*) A. M. Tafesh and J. Weiguny, *Chem. Rev.*, 1996, **96**, 2035; (*c*) E. Boymans, S. Boland, P. T. Witte, C. Müller and D. Vogt, *ChemCatChem*, 2013, **5**, 431.
5 (*a*) J. Lee, D. H. K. Jackson, T. Li, R. E. Winans, J. A. Dumesic, T. F. Kuech and G. W. Huber, *Energy Environ. Sci.*, 2014, **7**, 1657; (*b*) Z. Wei, J. Wang, S. Mao, D. Su, H. Jin, Y. Wang, F. Xu, H. Li and Y. Wang, *ACS Catal.*, 2015, **5**, 4783; (*c*) R. V. Jagadeesh, A.-E. Surkus, H. Junge, M.-M. Pohl, J. Radnik, J. Rabeah, H. Huan, V. Schünemann, A. Brückner and M. Beller, *Science*, 2013, **342**, 1073; (*d*) R. K. Rai, A. Mahata, S. Mukhopadhyay, S. Gupta, P.-Z. Li, K. T. Nguyen, Y. Zhao, B. Pathak and S. K. Singh, *Inorg. Chem.*, 2014, **53**, 2904.
6 (*a*) J. R. Long and O. M. Yaghi, *Chem. Soc. Rev.*, 2009, **38**, 1213; (*b*) H.-C. Zhou, J. R. Long and O. M. Yaghi, *Chem. Rev.*, 2012, **112**, 673; (*c*) H.-C. Zhou and S. Kitagawa, *Chem. Soc. Rev.*, 2014, **43**, 5415.
7 (*a*) T. K. Kim, K. J. Lee, J. Y. Cheon, J. H. Lee, S. H. Joo and H. R. Moon, *J. Am. Chem. Soc.*, 2013, **135**, 8940; (*b*) S. Ma, G. A. Goenaga, A. V. Call and D.-J. Liu, *Chem. – Eur. J.*, 2011, **17**, 2063; (*c*) Y.-X. Zhou, Y.-Z. Chen, L. Cao, J. Lu and H.-L. Jiang, *Chem. Commun.*, 2015, **51**, 8292; (*d*) Y.-Z. Chen, C. Wang, Z.-Y. Wu, Y. Xiong, Q. Xu, S.-H. Yu and H.-L. Jiang, *Adv. Mater.*, 2015, **27**, 5010; (*e*) S. Zhao, H. Yin, L. Du, L. He, K. Zhao, L. Chang, G. Yin, H. Zhao, S. Liu and Z. Tang, *ACS Nano*, 2014, **8**, 12660; (*f*) W. Zhong, H. Liu, C. Bai, S. Liao and Y. Li, *ACS Catal.*, 2015, **5**, 1850; (*g*) W. Xia, A. Mahmood, R. Zou and Q. Xu, *Energy Environ. Sci.*, 2015, **8**, 1837–1866; (*h*) B. Liu, H. Shioyama, T. Akita and Q. Xu, *J. Am. Chem. Soc.*, 2008, **130**, 5390; (*i*) E. Kim and M. Yoon, *J Porous Mater.*, 2015, **22**, 1495; (*j*) X. Yang, Y.-B. Tang, X. Huang, H. T. Xue, W. P. Kai, W. Y. Li, T.-W. Ng and C.-S. Lee, *J. Power Sources*, 2015, **284**, 109; (*k*) F. Zheng, M. He, Y. Yang and Q. Chen, *Nanoscale*, 2015, **7**, 3410; (*l*) A. Banerjee, V. Aravindan, S. Bhatnagar, D. Mhamane, S. Madhavi and S. Ogale, *Nano Energy*, 2013, **2**, 890; (*m*) J.-D. Xiao, L.-G. Qiu, X. Jiang, Y.-J. Zhu, S. Ye and X. Jiang, *Carbon*, 2013, **59**, 372; (*n*) G. Huang, F. Zhang, L. Zhang, X. Du, J. Wang and L. Wang, *J. Mater. Chem. A*, 2014, **2**, 8048.
8 (*a*) S. Surblé, C. Serre, C. Mellot-Draznieks, F. Millange and G. Férey, *Chem. Commun.*, 2006, 284; (*b*) H. J. Lee, W. Cho, E. Lim and M. Oh, *Chem. Commun.*, 2014, **50**, 5476.
9 (*a*) K. Woo, H. J. Lee, J. P. Ahn and Y. S. Park, *Adv. Mater.*, 2003, **15**, 1761; (*b*) D.-H. Liu, Y. Guo, L.-H. Zhang, W.-C. Li, T. Sun and A.-H. Lu, *Small*, 2013, **9**, 3852.
10 M. Descostes, F. Mercier, N. Thromat, C. Beaucaire and M. Gautier-Soyer, *Appl. Surf. Sci.*, 2000, **165**, 288.

